The partial dissociation of MHC class I bound peptides exposes their N terminus to trimming by endoplasmic reticulum aminopeptidase 1

Athanasios Papakyriakou[1,2,*], Emma Reeves[2,3,*], Mary Beton[1,2], Halina Mikolajek[1,2], Leon Douglas[2], Grace Cooper[2,3], Tim Elliott[2,3], Jörn M. Werner[1,2], Edward James[2,3]

From the [1]Centre for Biological Sciences, Faculty of Natural & Environmental Sciences, University of Southampton, UK; [2]Institute for Life Sciences, University of Southampton, Southampton, UK; [3]Centre for Cancer Immunology, University of Southampton Faculty of Medicine, University Hospital Southampton, Southampton, UK

Running Title: *ERAP1 trimming of MHC I-bound peptides*

* Both authors contributed equally to the manuscript

To whom correspondence should be addressed: Edd James, Centre for Cancer Immunology, University of Southampton Faculty of Medicine, University Hospital Southampton, Tremona Road, Southampton, SO16 6YD, UK, Telephone: (+44) 2381204309; FAX (+44) 2381205152; Email: eddjames@soton.ac.uk

ABSTRACT

Endoplasmic reticulum aminopeptidase 1 (ERAP1) and ERAP2 process N-terminally extended antigenic precursors for optimal loading onto major histocompatibility complex class I (MHC I) molecules. We and others have demonstrated that ERAP1 processes peptides bound to MHC I, but the underlying mechanism is unknown. To this end, we utilized single-chain trimers (SCT) of the ovalbumin-derived epitope SIINFEKL (SL8) tethered to the H2-K^b MHC I determinant from mouse and introduced three substitutions, E63A, K66A, and W167A, at the A-pocket of the peptide-binding groove in the MHC I heavy chain, which interact with the N termini of peptides. These variants significantly decreased SL8-presenting SCT at the cell surface in the presence of ERAP1, but did not affect overall SCT expression, indicating that ERAP1 trims the SL8 N terminus. Comparison of the X-ray crystal structures of WT and three variant SCTs revealed only minor perturbations of the peptide-binding domain in the variants. However, molecular dynamics simulations suggested that SL8 can dissociate partially within a sub-microsecond timescale, exposing its N terminus to the solvent. We also found that the C terminus of MHC I–bound SL8 remains deeply buried in the F-pocket of MHC I.

Furthermore, free-energy calculations revealed that the three SCT variants exhibit lower free-energy barriers of N terminus dissociation than the WT K^b. Taken together, our results are consistent with a previously observed model in which the partial dissociation of bound peptides from MHC I exposes their N terminus to trimming by ERAP1, while their C terminus is anchored at the F-pocket.

Major histocompatibility complex class I (MHC I) molecules present a diverse array of antigenic peptides, the so-called immunopeptidome, to circulating cytotoxic T lymphocytes. MHC I are heterotrimers consisting of a transmembrane heavy chain (HC), β_2-microglobulin (β_2m) and a peptide antigen, typically of 8–11 amino acids in length. These peptides originate from self-proteins including aberrantly expressed cancer antigens as well as foreign proteins from intracellular pathogens. The precise composition of the immunopeptidome and its ability to shape the antigen-specific T cell response to both infections and cancer are thus central to the mechanism of immunosurveillance.

The antigen processing pathway consists of a number of sequential steps and editing events to ensure complete and stable assembly of peptide-

MHC I (pMHC I) complexes in the endoplasmic reticulum (ER) and their expression at the cell surface. Antigenic precursors are generated from larger protein fragments by the (immuno)proteasome and may undergo further processing by cytosolic proteases (1-3). The resulting peptides often contain families of N-terminally extended precursors which require further processing before they can bind to MHC I with high affinity (2-4). These precursors are transported into the ER lumen by the transporter associated with antigen processing (TAP) with a preference for 8-12mer peptides (5,6). Here, endoplasmic reticulum aminopeptidase 1 (ERAP1) and ERAP2, trim peptides to the optimal length for stable MHC I binding in the final editing step of the antigen processing pathway (7-9). The peptide loading complex (PLC) in the ER orchestrates peptide transport and the assembly of newly synthesized MHC I with high affinity peptides; a process that is tightly regulated by the peptide editing function of tapasin (Tpn), resulting in the preferential egress to the cell surface of stable pMHC I (10). The editing functions of ERAP1/2 and Tpn are synchronised spatiotemporally, although no physical interaction between ERAP1/2 and Tpn has yet been established.

The trimming function of ERAP1 shapes the immunopeptidome; genetic knock-out of ERAP1 (ERAAP in mice) reduces the level of MHC I expression at the cell surface by up to 70% in mice and 10% in humans, depending on the MHC I allele (7,11). This loss of ERAP1 function gives rise to fewer peptides that are longer in length (12,13). The resultant change in repertoire can initiate a strong CTL response *in vivo* if ERAAP KO cells are injected into ERAAP competent mice, indicating the ability of ERAAP/ERAP1 to control the epitope specificity of CTL responses (14). In accordance with TAP transport, ERAP1 has a substrate length preference of 10-16mer peptides (15) and trims different amino acid residues from the N-terminus of precursor peptides at different rates thereby forming a distinct hierarchy of N-terminal extension preferences (16,17). Through the combined action on candidate peptides of N-terminal trimming and MHC I binding, the dominant products are peptides of 8-10 amino acids, which is generally optimal for forming stable pMHC I complexes. Importantly, ERAP1 is also able to "overtrim" peptides resulting in the

destruction of some epitopes (11,18,19). This specificity in turn shapes the abundance of peptides presented, and can affect the magnitude of T cell responses to pathogens and cancer (18,20). Thus, ERAP1 is a key regulator of peptide generation and presentation to CTL.

In humans, ERAP1 is highly polymorphic, with single nucleotide polymorphisms (SNPs), associated with a number of autoimmune diseases and cancer (21-24). SNPs in ERAP1 form discrete allotypes, which are associated with different trimming specificities broadly categorized into efficient, hypoactive and hyperactive phenotypes. Allotype-dependent ERAP1 trimming activity affects the peptide repertoire and the level of MHC I at the cell surface, and these activities combine in heterozygotes (17,25). The structural basis for the differences in function due to the SNPs is not clear. Some polymorphic sites may interact with parts of the active site, an obvious target for altered function, whilst others may interfere with the dynamics of the "open" and "closed" conformation (26-28). However, the majority of polymorphic residues are not located within the active site or inter-domain junctions, and are harder to reconcile with function.

The precise mechanism by which ERAP1 trims N-terminal amino acids remains unclear. Although ERAP1 has not been shown to interact directly with the PLC, studies have identified the requirement of MHC I for ERAP1 peptide trimming, resulting in destruction of the epitope when the correct MHC I is absent (29). Interestingly, we and others have shown the ability of ERAP1 to process peptides bound to MHC I (17,30). This suggests that the substrate for ERAP1 could be a pMHC I complex in which: a) the peptide N-terminus is permanently or occasionally exposed to the ERAP1 active site as a result of N-terminal extension out of the A-pocket of the peptide binding groove (in which the N-terminus of bound peptides are buried in the native pMHC I structure), or b) suboptimal docking of the peptide N-terminus with the binding groove. A complementary or alternative hypothesis has been suggested, supported by *in vitro* and crystallographic studies, where ERAP1 acts as the "molecular ruler" by binding both the N- and C-terminus of a free peptide within an internal substrate binding channel (27,31).

To establish proof of principle that the ability of ERAP1 to trim MHC I-bound peptide was dependent on an exposed N-terminus we investigated ERAP1 peptide trimming after mutating the MHC I A-pocket in such a way as to reduce the likelihood of it forming stable interactions with the N-terminus of bound peptide and protecting it from trimming. We show that pMHC I complexes with single point mutations at key peptide-interacting residues in the A-pocket, and engineered for enhanced binding to peptide at its C-terminus, results in greater susceptibility to ERAP1 overtrimming.

RESULTS

Mutation of A-pocket residues enhances ERAP1 dependent trimming of bound peptide

ERAP1 has been shown to trim peptides bound to MHC I, however the precise mechanism by which this occurs is still unknown. Nevertheless, these studies suggest that MHC I may act as a molecular template for trimming of peptides to the correct length for presentation, and may be regulated by the relative kinetics of ERAP1 trimming versus A-pocket binding for a peptide bound in the peptide binding groove (17,30). A greater understanding of the mechanism that underpins the trimming of MHC I bound peptide may help to interpret the observed variations in activity between ERAP1 allotypes, including overtrimming, which are harder to accommodate within the ERAP1 molecular ruler hypothesis.

Based on an examination of the native structure of the SIINFEKL (SL8)/K^b pMHC I complex (32), and the structure of the single-chain SL8-β_2m-K^b heavy chain (HC) trimer (33), we introduced alanine substitutions at residues, 63, 66 and 167 in the MHC I HC which interact with the bound peptide in the A-pocket. Positions E63 and K66 interact directly with S(P_1) and I(P_2) of SL8, while W167 caps off the N-terminus amino group of the peptide ((32,33) and Supplemental Fig. S1). Alanine substitutions at the three K^b residues would be expected to significantly reduce the number of hydrogen bonds and van der Waal contacts between the peptide and peptide binding groove, thus reducing the binding affinity of the N-terminus of SL8 to the A-pocket of K^b. In order to avoid complications arising from consequent lowering of the macroscopic off-rate, we utilized a disulfide-linked SL8/K^b single chain construct (WT-SCT,

Fig. 1). The construct consists of SL8 peptide linked with β_2m and K^b HC in which the C-terminus of SL8 is tethered to the K^b binding groove through a disulfide bond between Y84C of K^b and a second cysteine within the peptide-β_2m linker (Fig. 1*B* and *C* and (34)).

We have previously demonstrated that the WT-SCT can be trimmed to IINFEKL/K^b (IL7-SCT) by a hyperfunctional ERAP1 variant using mass spectrometric analysis (17). Another way of detecting this trimming event is to use recognition of the pMHC I complex by the 25-D1.16 antibody, which is specific for the SL8/K^b complex and recognizes WT-SCT (35). We confirmed this reactivity and in addition showed that 25-D1.16 did not recognize IL7-SCT when transfected into HeLa cells despite being expressed at similar levels to the WT-SCT control, as detected by anti-mouse β_2M antibody (Fig. 2*A*). This indicated that 25-D1.16 reactivity could be used as an indirect measure of ERAP1 dependent N-terminal trimming of MHC bound SL8 in the WT-SCT, offering a convenient way to determine whether mutations in the A-pocket of K^b permitted "overtrimming" of its peptide cargo by ERAP1.

In order to evaluate the impact of mutating A-pocket side-chains on the N-terminal trimming by ERAP1, we first generated an ERAP1 knockout in HeLa cells using CRISPR/Cas9 (HeLa E1KO). This approach resulted in cells expressing no detectable ERAP1 protein (Fig. 2*B*). Transfection of HeLa E1KO with WT-SCT or each of the three variant SCT resulted in their expression at the cell surface at similar levels measured by 25-D1.16 (Fig. 2*C*). This confirmed that mutation of the A-pocket does not affect the ability of the variants to fold in the ER and egress to the cell surface, which is consistent with the observation that there is no interaction between 25-D1.16 and E63, K66 or W167 in the crystal structure of the SL8/K^b/25-D1.16 complex (36).

To confirm that the A-pocket mutations did not disrupt the general architecture of the peptide binding groove of K^b, we determined the structures of WT-SCT (Fig. 1) and its three alanine-substituted variants by X-ray crystallography. The structures were resolved to a resolution range of 1.90–2.40 Å (Table 1) and showed the same topologies for β_2m, α_3 and peptide binding domains. In line with the structural similarity of the backbone between WT and variants, the previously identified

hydrogen bonds between: i) the terminal amine of $S(P_1)$ and the phenolic groups of Y7 and Y171, ii) the backbone carbonyl of $S(P_1)$ and the phenolic group of Y159 and iii) the amide of $I(P_2)$ with a structurally conserved water molecule, (Wat1), remain preserved in all variants (Fig. 3). A hydrogen bond between the $S(P_1)$ hydroxyl group and the side chain carboxylate group of E63 is detected in WT-, W167A-, and K66A-SCT, but not in the E63A-SCT variant (Fig. 3*B*). Similarly, the hydrogen bond between the backbone carbonyl group of $I(P_2)$ and the side-chain amine of K66, present in WT-, E63A- and W167-SCT, is not present in K66A-SCT (Fig. 3*C*). The space created by the shorter A66 side-chain is occupied by two water molecules, one of which is stabilized by a hydrogen bond with the carbonyl group of $I(P_2)$. For the W167A-SCT variant the structure and H-bonding network around $S(P_1)$ and $I(P_2)$ remain very similar to WT-SCT, while the space created by the missing W167 indole ring is filled by three water molecules (Fig. 3*D*). Despite the loss of hydrogen bonds, there was little variation in the peptide conformation and the interacting residues of the peptide binding groove varied very little; the only obvious differences being in the orientation of the side chains of K66 and $N(P_4)$ in the E63A-SCT (Fig. 3*B*). Interestingly, the side chain of $N(P_4)$ adopted similar orientation in K66A-SCT, while two alternative rotamer states of the $N(P_4)$ side chain were resolved in W167A-SCT (Fig. 3*C* and *D*). Such side chain rearrangements, though minor, are suggestive of an increased flexibility in SL8 within the peptide binding groove.

In light of the similarities in overall structure and the likelihood that the selected mutations at positions 63, 66 or 167 result in weakened interactions between the peptide N-terminus and MHC I, we proceeded to measure the impact of co-expressing ERAP1 with the variants on their cell surface expression and reactivity to 25-D1.16. Expression of wild-type (*002) ERAP1 (25) in SCT transfected HeLa E1KO resulted in a significant decrease in the levels of all A-pocket variants detected by 25-D1.16 (~35-40%; Fig. 4*A* and *B*). By contrast, no difference in the levels of WT-SCT was observed when ERAP1 was expressed (Fig. 4*A* and *B*). As expected, cell surface levels of all SCT variants in the presence of ERAP1, determined by anti-mouse β_2M antibody was similar, confirming that the reduction in 25-

D1.16 staining was likely due to trimming of SL8 to IL7 and not due to decreased levels of SCT at the cell surface. This showed that mutation of the A-pocket increased the ability of ERAP1 to trim SCT linked peptide, and indicated a link between A-pocket/peptide affinity and ERAP1 trimming of the N-terminus.

ERAP1 trimming of SCT reduces detection by B3Z T cells

To determine the effect of introducing the A-pocket mutations on antigen presentation to T cells we utilized B3Z T cell hybridomas. B3Z recognizes SL8 but not IL7 (Supplemental Fig. S2 and (37)), and therefore illustrates how peptide overtrimming by ERAP1 can alter T cell responses to a dominant antigen. Unlike 25-D1.16, the B3Z T cell receptor was sensitive to mutations in the A-pocket, as all three variants were recognized less well compared to WT-SCT when transfected into HeLa E1KO, despite their equivalent expression at the cell surface (Figs. 4*A* and 5*A*). This disruption could be due to alteration of TcR contact regions not shared by the 25-D1.16 antibody (32,38), either directly or indirectly, which is mediated via side chain rearrangement in K^b HC or SL8. In particular, the observed changes in the orientation of $N(P_4)$ side chains in the variants (Fig. 3) are consistent with previous observations that anti-SL8 TcRs are sensitive to alterations at P_4, P_6 and P_7 (39). The least affected variant was E63A-SCT, so we examined whether the ability of this variant to stimulate B3Z when ERAP1 was expressed. In the presence of ERAP1, E63A-SCT showed a significant reduction in B3Z stimulation (~35%), consistent with trimming of SL8 to IL7 (Fig. 5*A* and *B*). By contrast, WT-SCT showed very little difference in B3Z stimulation when ERAP1 was present (Fig. 5*A* and *B*). This difference was even detected against a background of endogenous ERAP1 expression in HeLa cells, where we observed a reduction in B3Z stimulation for both WT- and E63A-SCT after transfection of ERAP1, with the effect being most pronounced for the variant (~35% reduction compared to ~15% reduction; Fig. 5*C*).

Molecular dynamics simulations

The crystallographic and antigen presentation results indicate that although A-pocket mutations do not affect the overall structure of SCT,

4

they still promote overtrimming of SL8 to IL7 by ERAP1. In order to investigate the possible mechanism underpinning this observation, we employed molecular dynamics (MD) simulations to examine the effect on dynamics of the WT- and variant SCT at the ns to μs timescale. The all-atom MD simulations were initiated from the coordinates of our four X-ray structures and were performed in explicit solvent for a total time of 0.51 μs for each system. To examine the effect of the linker on the dynamics of K^b, we also carried out MD simulations after removing the PL linker between the SL8 and β$_2$m. These calculations were performed using similar initial coordinates, simulation parameters and total time for each system.

The peptide binding domain of WT-SCT displayed remarkable stability as evidenced by the root mean squared deviation (RMSD) of the corresponding $C^α$ atoms with respect to the X-ray structure (Supplemental Fig. S3*A*). The average value of 1.2 ± 0.1 Å suggests that the overall structure of the WT-SCT fluctuates around the crystallographic coordinates at the simulation timescale. By contrast, the SCT variants exhibited higher RMSD values of 1.7-1.8 ± 0.2–0.3 Å, a first indication of the effect of the mutated residues on the conformational dynamics of the antigen-binding groove. The peptide in both E63A- and K66A-SCT displayed low $RMSD^{Cα}$ values (< 1.0 Å), whereas SL8 in W167A-SCT deviated more from the initial position, with $RMSD^{Cα}$ of approximately 2.0 Å (Supplemental Fig. S3*B*). In the untethered pMHC I (native and A-pocket mutants), the $RMSD^{Cα}$ in the peptide binding domain of K^b with respect to the crystallographic coordinates displayed similar values in the range of 1.3-1.4 Å (Supplemental Fig. S3*C*). This was also the case for the SL8 peptide atoms in WT-, E63A- and K66A-K^b, which deviated by 2-3 Å (Supplemental Fig. S3*D*). Remarkably, SL8 in W167A-K^b deviated significantly during the simulation and displayed $RMSD^{Cα}$ of 6.8 ± 1.1 Å.

Examination of the MD trajectory of the untethered W167A pMHC I revealed that the N-terminus of SL8 became detached from the A-pocket within 10 ns after equilibration of the system. Partial dissociation of the N-terminal portion of the peptide was observed, however complete dissociation did not occur at this timescale even when the anchor residue F(P$_5$), initially buried inside the binding groove, turned towards the solvent-exposed face of the groove (Supplemental Movie 1 and Fig. 6*A*), indicating the strong and preferential binding of the peptide C-terminus. Although the rare event of partial peptide unbinding at the sub-μs timescale was only observed in the simulation of the W167A-SCT, this does not mean that similar dissociation events cannot occur in other pMHC I.

Free energy calculations of the N-terminus dissociation

Partial peptide dissociations have previously been observed in MD studies of HLA-B*27:05 (40), HLA-A*02:01 (41), as well as in MD simulations of the HLA-B*44:02 loaded with peptides truncated or modified at the C- or N-terminus (42). In addition, a "flapping" behavior of both the N- or C-terminal regions of the peptides has been reported in a large scale MD study of HLA-B*08:01 in complex with 172 variants (single-point mutants) of the Epstein−Barr virus peptide FLRGRAYGL (43). These considerations prompted us to study the partial N-terminus dissociation pathway using free energy calculations. To investigate the effect of A-pocket mutations on the peptide dynamics, we employed the umbrella sampling method and extracted the free energy profiles of N-terminus partial dissociation for the WT-SCT and three variants. Umbrella sampling is performed through a series of restraint MD simulations that are carried out in small, overlapping steps (windows) along the pathway under study. In our case, the distance $δ$ between the $C^α$ atom of S(P$_1$) and the center at the bottom of the A-pocket was selected as the collective variable (Fig. 6*A*, Supplemental Fig. S4 and computational methods for details). Simulations were initiated as close as possible to the crystallographic coordinates of the four SCTs and a harmonic potential was used to bias the reaction coordinate $δ$ in 0.5 Å steps until the N-terminus of S(P$_1$) was completely exposed to the solvent. The free energy profiles (potentials of mean force) along the N-terminus dissociation pathway were obtained from weighted histogram analysis of the collected data (Fig. 6*B*). All three SCT variants displayed lower free energy barriers of dissociation with respect to the WT-SCT and in the order of 3-8 Kcal/mol. In particular, E63A-SCT exhibited the lowest free energy profile, followed

by W167A-SCT, both of which displayed the lowest energy barriers at the mid-points of the dissociation path. To confirm these observations and exclude the potential bias introduced by the linker and the presence of the disulfide bond tethering the C-terminus of the bound peptide, we calculated the corresponding potentials of the four SL8/K^b systems where the $C(P_{10})$ in the linker is removed untethering the peptide (Fig. 6C). These untethered SL8/K^b molecules exhibited comparable profiles to those observed for the tethered versions.

DISCUSSION

Using MHC I single chain trimers we identified that alanine substitution of A-pocket MHC I residues contacting the N-terminus of bound peptide resulted in ERAP1-dependent overtrimming of SL8 to IL7. Structures of these variants determined by X-ray crystallography showed that local side chain rearrangements of K^b and SL8 in the vicinity of the substituted residues in some cases retained favorable interactions between K^b and SL8 by including insertion of water molecules that preserved hydrogen bonds. Any reduction of peptide affinity due to weaker interaction between peptide N-terminus and the A-pocket variants was not evident from the crystal structures. However, MD simulations and free energy calculations of SCT and untethered pMHC I clearly showed a strong correlation between the A-pocket variants and the ability of the peptide N-terminus to partially dissociate and be accessible for ERAP1 trimming. Taken together, these data are consistent with the model proposed by Chen et al (30) in which the partial dissociation of bound peptides from MHC I exposes their N-terminus to trimming by ERAP1 while their C-terminus remains deeply buried in the F-pocket.

MD simulations showed that partial dissociation of the peptide from K^b occurred at the N-terminus with strong and preferential binding of the peptide C-terminus. This finding is supported by the greater increase in K_{off} rates for N-terminal compared to C-terminal truncated peptides from D^b (44). In addition, a recent combined experimental and computational study of K^b demonstrated the prominent role of the C-terminus in stabilization of the bound peptide and revealed that truncation of the peptide C-terminus results in high flexibility of the F-pocket region, similar to that of the empty groove (45). These observations are consistent with

the previously proposed model for trimming of N-terminally extended peptides where the C-terminus is anchored into the F-pocket of the binding groove and the N-terminus is available for trimming by ERAP1 (30).

In our experimental system, the increased stability afforded by tethering the peptide to MHC I has enabled observation of peptide trimming when bound to MHC I (17), but does not indicate whether it occurs during the normal processing of antigens. Chen et al recently showed that both tethered and free peptide bound to HLA-B*08:01 were substrates for ERAP, indicating that trimming of MHC I-bound peptides could be a physiologically relevant mechanism (30). In addition, consistent with our observations, a recent MD study of peptide bound to HLA-B*44:02 showed that removal of the N-terminal amino acid caused the dissociation of the P_2 amino acid, with further truncation leading to greater dissociation of the peptide from MHC I at the N-terminus (42). The weaker interaction of the peptide N-terminus predisposing to overtrimming and the greatly increased macroscopic dissociation rates of the resultant shorter peptides may therefore represent a quality control step similar to that for tapasin/PLC (46). This process would improve the half-life of pMHC I complexes at the cell surface through both generation of the correct peptide length and disposal of peptides that have poor N-terminal affinity.

The overtrimming of several epitopes by ERAP1 has been noted (11,18-20), and it is likely that the steady-state generation of any given epitope is a balance between overtrimming and MHC I binding and egress of the pMHC I complex to the cell surface. The destruction of epitopes has been demonstrated for minor histocompatibility antigens where knockout of ERAAP increased the quantity of presented epitope (11), and for viral antigens (20). We have shown that ERAP1 overtrimming can have a significant impact on anti-tumor immunity in a preclinical model, where reduction of ERAAP protein in the murine CT26 tumor significantly increased generation of the immunodominant cryptic epitope (18). In addition, Keller et al have shown that destruction of the immunodominant tumor antigen in melanoma, MART-1, by ERAP1 may affect the success of epitope-specific immunotherapy (19). These examples highlight the possibility of modulating of ERAP1 function therapeutically, for example with

small molecules (18,47) to enhance immunity. This is particularly pertinent in light of the fact that ERAP1 is functionally polymorphic in the human population (17), thus patients could be stratified according to their ERAP1 allotypes for their suitability to respond to targeted ERAP1 modulators. For example, patients expressing hyperactive ERAP1 might be likely to mount better responses to overtrimmed tumor derived epitopes if given ERAP1 inhibitors, and conversely those expressing hypoactive allotypes if given ERAP1 activators.

Quite how ERAP1 might gain access to the N-termini of partially dissociated MHC I-bound peptide substrates in such a way as to permit trimming to heptapeptide or shorter is unclear, and would require ERAP1 to adopt a conformation that is more open than observed in previously published crystal structures (26-28). Nevertheless, this study, when taken with other biological and structural data (29,30,42) indicate that ERAP1 can use the pMHC I complex as a substrate *in vitro* and *in vivo*, and that partial dissociation of MHC I bound peptides can expose them to overtrimming. It will be important to learn how structural differences between naturally occurring ERAP1 allotypes relate to their enzyme activity, and whether their recognition of pMHC I as a substrate is a contributing factor.

EXPERIMENTAL PROCEDURES

Generation of SCT constructs

A K^b/SL8 disulfide trap single-chain trimer (SCT) has been previously described (17). To generate the A-pocket variants, site directed mutagenesis of WT-SCT heavy chain amino acids at position E63, K66 and W167 to alanine residues was performed using the following primers (mutated nucleotides in italics); E63A 5′ CGTATTGGGAGCGGG*CC*ACACAGAAAGCC AAGG and 3′ CCTTGGCTTTCTGTGT*GG*CCCGCTCCCAAT ACG, K66A 5′ GGAGCGGGAGACACAG*GCC*GCCAAGGGC AATGAGC and 3′ GCTCATTGCCCTTGGC*GGC*CTGTGTCTCCC GCTCC and W167A 5′ GGCACGTGCGTGGAG*GC*GCTCCGCAGATA CCTG and 3′ CAGGTATCTGCGGAGC*GC*CTCCACGCACG TGCC.

Generation of ERAP1 deficient HeLa cells

ERAP1-deficient HeLa cells were generated using clustered regulatory interspaced short palindromic repeats associated protein 9 system (CRISPR/Cas9) according to (25). ERAP1 knockdown was determined by immunoblot and successful clones were expanded and cultured.

Cell lines, transfection, flow cytometry and T cell activation

HeLa and HeLa EKO cell lines were maintained in RPMI-1640 culture medium supplemented with 10% FCS, 2 mM L-glutamine, 1 mM sodium pyruvate and 50 U/mL penicillin/streptomycin. B3Z T cell hybridoma (a kind gift from Prof. N. Shastri, University of California, Berkeley, CA) was cultured as previously described (8). HeLa and HeLa E1KO cells were transfected with 1 μg of each of the SCT constructs WT-SCT, IL7-SCT, E63A-SCT, K66A-SCT and W167A-SCT, alongside either 1 μg ERAP1-pcDNA3.1 (previously described in (17)) or empty vector (pcDNA3.1) control using Fugene6 (Roche). After 48 hours, cell were harvested and assessed for SL8/K^b cell surface presentation by either flow cytometry or B3Z T cell activation. For cell surface expression of SCT, transfected HeLa or HeLa Eko cells were stained for SL8/K^b (25-D1.16-FITC) and mouse anti-mouse β_2m (S19.8, BD biosciences; 555299) and analysed by flow cytometry using BD FACS Canto II and FlowJo analysis software (TreeStar). For T cell activation, transfected cells were incubated overnight with the *LacZ* inducible T cell hybridoma, B3Z, and assessed as described in (17).

Immunoblotting

Expression of ERAP1 was determined by immunoblot. Both HeLa and HeLa Eko, transfected with and without ERAP1, were lysed in 0.5% Nonidet P-40, 150 mM NaCl, 5 mM EDTA and 20 mM Tris pH 7.4, supplemented with PMSF and iodoacetamide (Sigma-Aldrich). Proteins were separated by 10% SDS-PAGE and transferred to a nitrocellulose membrane (GE healthcare). Immunoblots were probed with primary antibodies, goat anti-human ARTS1 (R&D systems; AF2334) or mouse anti-GAPDH (Abcam; Ab8245) followed by HRP-conjugated secondary antibodies. Protein expression was determined using SuperSignal West

pico or femto chemiluminscent substrate (Thermo-Fisher).

Expression of single-chain trimers

Disulfide-trap SIINFEKL/K^b single chain trimers (WT-SCT; a kind gift from Prof. Ted Hansen) were cloned and expressed in BL21 E. coli using standard procedures. The expressed protein was purified from inclusion bodies, resolubilized in 8 M urea and refolded through rapid dilution at 4°C (48). Concentrated refolded SCT were purified using size exclusion chromatography, his-tag purification and anion exchange and stored in HEPES buffer.

Determination of crystal structures

SCTs were crystallized with sitting drop vapor diffusion using a previously described screen for pMHC I crystallization (49). After cryoprotection with 30% v/v glycerol, crystals were frozen at 100 K and taken to beamlines IO4 and I24 at the Diamond Light Source, Oxford, UK, for collection of x-ray diffraction data. Data were processed with the automated Diamond xia2 software (50) and the CCP4 suite (51). Molecular replacement was performed with MOLREP using PDB coordinates 2QRI (33) for the WT-SCT, E63A-SCT and K66A-SCT structures, and the solved structure of E63A-SCT for W167A-SCT molecular replacement. Refinement was carried out in PHENIX (52) and subsequent rounds of model building using COOT (53). Optimal hydrogen bonding was calculated using the WHAT_IF server (54). The structures were deposited on PDB with accession codes 5OQF (WT-SCT), 5OQI (E63A-SCT), 5OQH (K66A-SCT) and 5OQG (W167A-SCT).

Computational methods

The four disulfide-trapped single-chain MHC I simulation systems were based on the crystallographic structures described herein. Only protein atoms were retained and the unresolved residues of the linker between the peptide and the β_2m (G14–S23) were modeled on the basis of the SL8-SCT (Y84C) structure determined previously (PDB ID: 2QRT) (33). The second linker between the C-terminus of β_2m and the N-terminus of the heavy chain was not modelled as it is not resolved in any X-ray structure to data and is not expected to affect the peptide dynamics significantly. Four

untethered SL8/K^b complexes were prepared by removing all atoms of residues G9–S13 of the linker that were resolved from the corresponding crystal structure of the SCT, and then the engineered Y84C was changed back to tyrosine.

Hydrogen atoms were added after calculating the protonation state of the ionizable groups at physiological pH (7.4) using the H++ v3.1 server with default parameters at pH 7.4 (55). In particular, histidine residues 3 and 93 of the heavy chain were set as positively charged, H68 of β_2m was protonated at $N^{\delta 1}$, whereas all other histidine residues were protonated at $N^{\epsilon 2}$. The proteins were solvated into truncated octahedral boxes with TIP3P waters extending up to 12 Å around the solute; the appropriate number of Na^+ and Cl^- ions was added so as to neutralize the total charge of each system and simulate an ionic strength of 0.15 M, and the AMBER *ff14SB* force field parameters (56) were applied.

Molecular dynamics simulations were performed with the GPU-accelerated version of PMEMD (57) at the Iridis4 supercomputer facility (University of Southampton). The MD parameters and equilibration protocol employed were the same as described in (58). Production runs were performed for 500 ns for each system in the NPT ensemble (*T*=300 K, *P*=1 bar). Trajectory snapshots were collected every 2 ps for further processing excluding the initial 10-ns equilibration period. Visual inspection of the trajectories and rendering of figures and movies was performed with VMD v1.9.3 (59).

Umbrella sampling calculations were performed for the four SCTs and the four untethered SL8/K^b systems. The potential of mean force (PMF) of the peptide N-terminus dissociation was calculated using harmonic distance restraints between the C^α atom of the N-terminal S(P_1) and the center of mass of the C^α atoms of residues 5, 6, 7, 26, 27, 28, 99, 100 and 101 at the base of the A-pocket (Supplemental Fig. S4). The reaction coordinate (δ) was divided in 16 windows of 0.5 Å steps, starting from δ=10 Å until complete dissociation of the N-terminal residue at δ=17.5 Å. Calculations were initiated from the solvent equilibrated systems at 1 ns and before releasing the positional restraints on the C^α atoms, so as all systems are as close as possible to the experimental structures. Equilibration was carried out for 5 ns in each window and the structure obtained at the last

8

frame was used as the starting structure of the subsequent window. Four independent MD simulations of 5 ns were performed in each window with force constants adjusted empirically so as to reach convergence of the resulting PMFs within at least 1 Kcal/mol and obtain a satisfactory overlap of the reaction coordinate distributions between adjacent windows (Supplemental Fig. S5). In cases where convergence was not satisfactory due to large conformational space that was not sampled, simulations were extended to 10 ns. The unbiased probability distributions of the distances and the PMF were obtained using the weighted histogram analysis method (60) with convergence tolerance of 0.001 Å. The errors at each point in the PMF plots were calculated as the standard deviation from the four independent production sets.

Statistical analysis

Two-way paired students' *t* test was performed for analysis of differences between experimental groups (GraphPad prism, www.graphpad.com).

Conflict of interest: The authors declare that they have no conflicts of interest with the contents of this article.

Author contributions: A.P. performed the molecular dynamics and free energy calculations. E.R. conducted the antigen presentation experiments. M.B. and H.M. performed crystallization of the proteins and solved the X-ray structures, L.D. and G.C. generated the SCT constructs and protein and conducted experiments, J.M.W., T.E. and E.J. conceived the project and supervised the work. The manuscript was written through contributions of all authors and all authors have given approval to the final version of the manuscript.

REFERENCES

1. Attaya, M., Jameson, S., Martinez, C. K., Hermel, E., Aldrich, C., Forman, J., Lindahl, K. F., Bevan, M. J., and Monaco, J. J. (1992) Ham-2 corrects the class I antigen-processing defect in RMA-S cells. *Nature* **355**, 647-649

2. Cascio, P., Hilton, C., Kisselev, A. F., Rock, K. L., and Goldberg, A. L. (2001) 26S proteasomes and immunoproteasomes produce mainly N-extended versions of an antigenic peptide. *EMBO J* **20**, 2357-2366

3. Kunisawa, J., and Shastri, N. (2003) The group II chaperonin TRiC protects proteolytic intermediates from degradation in the MHC class I antigen processing pathway. *Mol Cell* **12**, 565-576

4. Kunisawa, J., and Shastri, N. (2006) Hsp90alpha chaperones large C-terminally extended proteolytic intermediates in the MHC class I antigen processing pathway. *Immunity* **24**, 523-534

5. Koopmann, J. O., Post, M., Neefjes, J. J., Hammerling, G. J., and Momburg, F. (1996) Translocation of long peptides by transporters associated with antigen processing (TAP). *Eur J Immunol* **26**, 1720-1728

6. Lehnert, E., and Tampe, R. (2017) Structure and Dynamics of Antigenic Peptides in Complex with TAP. *Front Immunol* **8**, 10

7. Saveanu, L., Carroll, O., Lindo, V., Del Val, M., Lopez, D., Lepelletier, Y., Greer, F., Schomburg, L., Fruci, D., Niedermann, G., and van Endert, P. M. (2005) Concerted peptide trimming by human ERAP1 and ERAP2 aminopeptidase complexes in the endoplasmic reticulum. *Nat Immunol* **6**, 689-697

8. Serwold, T., Gonzalez, F., Kim, J., Jacob, R., and Shastri, N. (2002) ERAAP customizes peptides for MHC class I molecules in the endoplasmic reticulum. *Nature* **419**, 480-483

9. York, I. A., Chang, S. C., Saric, T., Keys, J. A., Favreau, J. M., Goldberg, A. L., and Rock, K. L. (2002) The ER aminopeptidase ERAP1 enhances or limits antigen presentation by trimming epitopes to 8-9 residues. *Nat Immunol* **3**, 1177-1184

10. Williams, A. P., Peh, C. A., Purcell, A. W., McCluskey, J., and Elliott, T. (2002) Optimization of the MHC class I peptide cargo is dependent on tapasin. *Immunity* **16**, 509-520

11. Hammer, G. E., Gonzalez, F., Champsaur, M., Cado, D., and Shastri, N. (2006) The aminopeptidase ERAAP shapes the peptide repertoire displayed by major histocompatibility complex class I molecules. *Nat Immunol* **7**, 103-112

12. Blanchard, N., Kanaseki, T., Escobar, H., Delebecque, F., Nagarajan, N. A., Reyes-Vargas, E., Crockett, D. K., Raulet, D. H., Delgado, J. C., and Shastri, N. (2010) Endoplasmic reticulum aminopeptidase associated with antigen processing defines the composition and structure of MHC class I peptide repertoire in normal and virus-infected cells. *J Immunol* **184**, 3033-3042

13. Chen, L., Fischer, R., Peng, Y., Reeves, E., McHugh, K., Ternette, N., Hanke, T., Dong, T., Elliott, T., Shastri, N., Kollnberger, S., James, E., Kessler, B., and Bowness, P. (2014) Critical role of endoplasmic reticulum aminopeptidase 1 in determining the length and sequence of peptides bound and presented by HLA-B27. *Arthritis Rheumatol* **66**, 284-294

14. Hammer, G. E., Gonzalez, F., James, E., Nolla, H., and Shastri, N. (2007) In the absence of aminopeptidase ERAAP, MHC class I molecules present many unstable and highly immunogenic peptides. *Nat Immunol* **8**, 101-108

15. Saric, T., Chang, S. C., Hattori, A., York, I. A., Markant, S., Rock, K. L., Tsujimoto, M., and Goldberg, A. L. (2002) An IFN-gamma-induced aminopeptidase in the ER, ERAP1, trims precursors to MHC class I-presented peptides. *Nat Immunol* **3**, 1169-1176

16. Hearn, A., York, I. A., and Rock, K. L. (2009) The specificity of trimming of MHC class I-presented peptides in the endoplasmic reticulum. *J Immunol* **183**, 5526-5536

17. Reeves, E., Edwards, C. J., Elliott, T., and James, E. (2013) Naturally occurring ERAP1 haplotypes encode functionally distinct alleles with fine substrate specificity. *J Immunol* **191**, 35-43

18.   James, E., Bailey, I., Sugiyarto, G., and Elliott, T. (2013) Induction of protective antitumor immunity through attenuation of ERAAP function. *J Immunol* **190**, 5839-5846

19.   Keller, M., Ebstein, F., Burger, E., Textoris-Taube, K., Gorny, X., Urban, S., Zhao, F., Dannenberg, T., Sucker, A., Keller, C., Saveanu, L., Kruger, E., Rothkotter, H. J., Dahlmann, B., Henklein, P., Voigt, A., Kuckelkorn, U., Paschen, A., Kloetzel, P. M., and Seifert, U. (2015) The proteasome immunosubunits, PA28 and ER-aminopeptidase 1 protect melanoma cells from efficient MART-126-35 -specific T-cell recognition. *Eur J Immunol* **45**, 3257-3268

20.   York, I. A., Brehm, M. A., Zendzian, S., Towne, C. F., and Rock, K. L. (2006) Endoplasmic reticulum aminopeptidase 1 (ERAP1) trims MHC class I-presented peptides in vivo and plays an important role in immunodominance. *Proc Natl Acad Sci U S A* **103**, 9202-9207

21.   Genetic Analysis of Psoriasis, C., the Wellcome Trust Case Control, C., Strange, A., Capon, F., Spencer, C. C., Knight, J., Weale, M. E., Allen, M. H., Barton, A., Band, G., Bellenguez, C., Bergboer, J. G., Blackwell, J. M., Bramon, E., Bumpstead, S. J., Casas, J. P., Cork, M. J., Corvin, A., Deloukas, P., Dilthey, A., Duncanson, A., Edkins, S., Estivill, X., Fitzgerald, O., Freeman, C., Giardina, E., Gray, E., Hofer, A., Huffmeier, U., Hunt, S. E., Irvine, A. D., Jankowski, J., Kirby, B., Langford, C., Lascorz, J., Leman, J., Leslie, S., Mallbris, L., Markus, H. S., Mathew, C. G., McLean, W. H., McManus, R., Mossner, R., Moutsianas, L., Naluai, A. T., Nestle, F. O., Novelli, G., Onoufriadis, A., Palmer, C. N., Perricone, C., Pirinen, M., Plomin, R., Potter, S. C., Pujol, R. M., Rautanen, A., Riveira-Munoz, E., Ryan, A. W., Salmhofer, W., Samuelsson, L., Sawcer, S. J., Schalkwijk, J., Smith, C. H., Stahle, M., Su, Z., Tazi-Ahnini, R., Traupe, H., Viswanathan, A. C., Warren, R. B., Weger, W., Wolk, K., Wood, N., Worthington, J., Young, H. S., Zeeuwen, P. L., Hayday, A., Burden, A. D., Griffiths, C. E., Kere, J., Reis, A., McVean, G., Evans, D. M., Brown, M. A., Barker, J. N., Peltonen, L., Donnelly, P., and Trembath, R. C. (2010) A genome-wide association study identifies new psoriasis susceptibility loci and an interaction between HLA-C and ERAP1. *Nat Genet* **42**, 985-990

22.   Mehta, A. M., Jordanova, E. S., van Wezel, T., Uh, H. W., Corver, W. E., Kwappenberg, K. M., Verduijn, W., Kenter, G. G., van der Burg, S. H., and Fleuren, G. J. (2007) Genetic variation of antigen processing machinery components and association with cervical carcinoma. *Genes Chromosomes Cancer* **46**, 577-586

23.   Wellcome Trust Case Control, C., Australo-Anglo-American Spondylitis, C., Burton, P. R., Clayton, D. G., Cardon, L. R., Craddock, N., Deloukas, P., Duncanson, A., Kwiatkowski, D. P., McCarthy, M. I., Ouwehand, W. H., Samani, N. J., Todd, J. A., Donnelly, P., Barrett, J. C., Davison, D., Easton, D., Evans, D. M., Leung, H. T., Marchini, J. L., Morris, A. P., Spencer, C. C., Tobin, M. D., Attwood, A. P., Boorman, J. P., Cant, B., Everson, U., Hussey, J. M., Jolley, J. D., Knight, A. S., Koch, K., Meech, E., Nutland, S., Prowse, C. V., Stevens, H. E., Taylor, N. C., Walters, G. R., Walker, N. M., Watkins, N. A., Winzer, T., Jones, R. W., McArdle, W. L., Ring, S. M., Strachan, D. P., Pembrey, M., Breen, G., St Clair, D., Caesar, S., Gordon-Smith, K., Jones, L., Fraser, C., Green, E. K., Grozeva, D., Hamshere, M. L., Holmans, P. A., Jones, I. R., Kirov, G., Moskivina, V., Nikolov, I., O'Donovan, M. C., Owen, M. J., Collier, D. A., Elkin, A., Farmer, A., Williamson, R., McGuffin, P., Young, A. H., Ferrier, I. N., Ball, S. G., Balmforth, A. J., Barrett, J. H., Bishop, T. D., Iles, M. M., Maqbool, A., Yuldasheva, N., Hall, A. S., Braund, P. S., Dixon, R. J., Mangino, M., Stevens, S., Thompson, J. R., Bredin, F., Tremelling, M., Parkes, M., Drummond, H., Lees, C. W., Nimmo, E. R., Satsangi, J., Fisher, S. A., Forbes, A., Lewis, C. M., Onnie, C. M., Prescott, N. J., Sanderson, J., Matthew, C. G., Barbour, J., Mohiuddin, M. K., Todhunter, C. E., Mansfield, J. C., Ahmad, T., Cummings, F. R., Jewell, D. P., Webster, J., Brown, M. J., Lathrop, M. G., Connell, J., Dominiczak, A., Marcano, C. A., Burke, B., Dobson, R., Gungadoo, J., Lee, K. L., Munroe, P. B., Newhouse, S. J., Onipinla, A., Wallace, C., Xue, M., Caulfield, M., Farrall, M., Barton, A., Biologics in, R. A. G., Genomics Study Syndicate Steering, C., Bruce, I. N., Donovan, H., Eyre, S., Gilbert, P. D., Hilder, S. L., Hinks, A. M., John, S. L., Potter, C., Silman, A. J., Symmons, D. P., Thomson, W., Worthington, J., Dunger, D. B., Widmer, B., Frayling, T. M., Freathy, R. M., Lango, H., Perry, J. R., Shields, B. M., Weedon, M. N., Hattersley, A. T., Hitman,

G. A., Walker, M., Elliott, K. S., Groves, C. J., Lindgren, C. M., Rayner, N. W., Timpson, N. J., Zeggini, E., Newport, M., Sirugo, G., Lyons, E., Vannberg, F., Hill, A. V., Bradbury, L. A., Farrar, C., Pointon, J. J., Wordsworth, P., Brown, M. A., Franklyn, J. A., Heward, J. M., Simmonds, M. J., Gough, S. C., Seal, S., Breast Cancer Susceptibility, C., Stratton, M. R., Rahman, N., Ban, M., Goris, A., Sawcer, S. J., Compston, A., Conway, D., Jallow, M., Newport, M., Sirugo, G., Rockett, K. A., Bumpstead, S. J., Chaney, A., Downes, K., Ghori, M. J., Gwilliam, R., Hunt, S. E., Inouye, M., Keniry, A., King, E., McGinnis, R., Potter, S., Ravindrarajah, R., Whittaker, P., Widden, C., Withers, D., Cardin, N. J., Davison, D., Ferreira, T., Pereira-Gale, J., Hallgrimsdo'ttir, I. B., Howie, B. N., Su, Z., Teo, Y. Y., Vukcevic, D., Bentley, D., Brown, M. A., Compston, A., Farrall, M., Hall, A. S., Hattersley, A. T., Hill, A. V., Parkes, M., Pembrey, M., Stratton, M. R., Mitchell, S. L., Newby, P. R., Brand, O. J., Carr-Smith, J., Pearce, S. H., McGinnis, R., Keniry, A., Deloukas, P., Reveille, J. D., Zhou, X., Sims, A. M., Dowling, A., Taylor, J., Doan, T., Davis, J. C., Savage, L., Ward, M. M., Learch, T. L., Weisman, M. H., and Brown, M. (2007) Association scan of 14,500 nonsynonymous SNPs in four diseases identifies autoimmunity variants. *Nat Genet* **39**, 1329-1337

24.   Guerini, F. R., Cagliani, R., Forni, D., Agliardi, C., Caputo, D., Cassinotti, A., Galimberti, D., Fenoglio, C., Biasin, M., Asselta, R., Scarpini, E., Comi, G. P., Bresolin, N., Clerici, M., and Sironi, M. (2012) A functional variant in ERAP1 predisposes to multiple sclerosis. *PLoS One* **7**, e29931

25.   Reeves, E., Colebatch-Bourn, A., Elliott, T., Edwards, C. J., and James, E. (2014) Functionally distinct ERAP1 allotype combinations distinguish individuals with Ankylosing Spondylitis. *Proc Natl Acad Sci U S A* **111**, 17594-17599

26.   Kochan, G., Krojer, T., Harvey, D., Fischer, R., Chen, L., Vollmar, M., von Delft, F., Kavanagh, K. L., Brown, M. A., Bowness, P., Wordsworth, P., Kessler, B. M., and Oppermann, U. (2011) Crystal structures of the endoplasmic reticulum aminopeptidase-1 (ERAP1) reveal the molecular basis for N-terminal peptide trimming. *Proc Natl Acad Sci U S A* **108**, 7745-7750

27.   Nguyen, T. T., Chang, S. C., Evnouchidou, I., York, I. A., Zikos, C., Rock, K. L., Goldberg, A. L., Stratikos, E., and Stern, L. J. (2011) Structural basis for antigenic peptide precursor processing by the endoplasmic reticulum aminopeptidase ERAP1. *Nat Struct Mol Biol* **18**, 604-613

28.   Papakyriakou, A., and Stratikos, E. (2017) The Role of Conformational Dynamics in Antigen Trimming by Intracellular Aminopeptidases. *Front Immunol* **8**, 946

29.   Kanaseki, T., Blanchard, N., Hammer, G. E., Gonzalez, F., and Shastri, N. (2006) ERAAP synergizes with MHC class I molecules to make the final cut in the antigenic peptide precursors in the endoplasmic reticulum. *Immunity* **25**, 795-806

30.   Chen, H., Li, L., Weimershaus, M., Evnouchidou, I., van Endert, P., and Bouvier, M. (2016) ERAP1-ERAP2 dimers trim MHC I-bound precursor peptides; implications for understanding peptide editing. *Sci Rep* **6**, 28902

31.   Chang, S. C., Momburg, F., Bhutani, N., and Goldberg, A. L. (2005) The ER aminopeptidase, ERAP1, trims precursors to lengths of MHC class I peptides by a "molecular ruler" mechanism. *Proc Natl Acad Sci U S A* **102**, 17107-17112

32.   Fremont, D. H., Stura, E. A., Matsumura, M., Peterson, P. A., and Wilson, I. A. (1995) Crystal structure of an H-2Kb-ovalbumin peptide complex reveals the interplay of primary and secondary anchor positions in the major histocompatibility complex binding groove. *Proc Natl Acad Sci U S A* **92**, 2479-2483

33.   Mitaksov, V., Truscott, S. M., Lybarger, L., Connolly, J. M., Hansen, T. H., and Fremont, D. H. (2007) Structural engineering of pMHC reagents for T cell vaccines and diagnostics. *Chem Biol* **14**, 909-922

34.   Truscott, S. M., Lybarger, L., Martinko, J. M., Mitaksov, V. E., Kranz, D. M., Connolly, J. M., Fremont, D. H., and Hansen, T. H. (2007) Disulfide bond engineering to trap peptides in the MHC class I binding groove. *J Immunol* **178**, 6280-6289

35.   Lybarger, L., Yu, Y. Y., Miley, M. J., Fremont, D. H., Myers, N., Primeau, T., Truscott, S. M., Connolly, J. M., and Hansen, T. H. (2003) Enhanced immune presentation of a single-chain major

histocompatibility complex class I molecule engineered to optimize linkage of a C-terminally extended peptide. *J Biol Chem* **278**, 27105-27111

36. Mareeva, T., Martinez-Hackert, E., and Sykulev, Y. (2008) How a T cell receptor-like antibody recognizes major histocompatibility complex-bound peptide. *J Biol Chem* **283**, 29053-29059

37. Shastri, N., and Gonzalez, F. (1993) Endogenous generation and presentation of the ovalbumin peptide/Kb complex to T cells. *J Immunol* **150**, 2724-2736

38. Denton, A. E., Wesselingh, R., Gras, S., Guillonneau, C., Olson, M. R., Mintern, J. D., Zeng, W., Jackson, D. C., Rossjohn, J., Hodgkin, P. D., Doherty, P. C., and Turner, S. J. (2011) Affinity thresholds for naive CD8+ CTL activation by peptides and engineered influenza A viruses. *J Immunol* **187**, 5733-5744

39. Jameson, S. C., and Bevan, M. J. (1992) Dissection of major histocompatibility complex (MHC) and T cell receptor contact residues in a Kb-restricted ovalbumin peptide and an assessment of the predictive power of MHC-binding motifs. *Eur J Immunol* **22**, 2663-2667

40. Omasits, U., Knapp, B., Neumann, M., Steinhauser, O., Stockinger, H., Kobler, R., and Schreiner, W. (2008) Analysis of key parameters for molecular dynamics of pMHC molecules. *Molecular Simulation* **34**, 781-793

41. Knapp, B., Demharter, S., Deane, C. M., and Minary, P. (2016) Exploring peptide/MHC detachment processes using hierarchical natural move Monte Carlo. *Bioinformatics* **32**, 181-186

42. Fisette, O., Wingbermuhle, S., and Schafer, L. V. (2017) Partial Dissociation of Truncated Peptides Influences the Structural Dynamics of the MHCI Binding Groove. *Front Immunol* **8**, 408

43. Knapp, B., and Deane, C. M. (2016) T-Cell Receptor Binding Affects the Dynamics of the Peptide/MHC-I Complex. *J Chem Inf Model* **56**, 46-53

44. Cerundolo, V., Elliott, T., Elvin, J., Bastin, J., Rammensee, H. G., and Townsend, A. (1991) The binding affinity and dissociation rates of peptides for class I major histocompatibility complex molecules. *Eur J Immunol* **21**, 2069-2075

45. Abualrous, E. T., Saini, S. K., Ramnarayan, V. R., Ilca, F. T., Zacharias, M., and Springer, S. (2015) The Carboxy Terminus of the Ligand Peptide Determines the Stability of the MHC Class I Molecule H-2Kb: A Combined Molecular Dynamics and Experimental Study. *PLoS One* **10**, e0135421

46. Howarth, M., Williams, A., Tolstrup, A. B., and Elliott, T. (2004) Tapasin enhances MHC class I peptide presentation according to peptide half-life. *Proc Natl Acad Sci U S A* **101**, 11737-11742

47. Zervoudi, E., Saridakis, E., Birtley, J. R., Seregin, S. S., Reeves, E., Kokkala, P., Aldhamen, Y. A., Amalfitano, A., Mavridis, I. M., James, E., Georgiadis, D., and Stratikos, E. (2013) Rationally designed inhibitor targeting antigen-trimming aminopeptidases enhances antigen presentation and cytotoxic T-cell responses. *Proc Natl Acad Sci U S A* **110**, 19890-19895

48. Mitaksov, V., and Fremont, D. H. (2006) Structural definition of the H-2Kd peptide-binding motif. *J Biol Chem* **281**, 10618-10625

49. Bulek, A. M., Madura, F., Fuller, A., Holland, C. J., Schauenburg, A. J., Sewell, A. K., Rizkallah, P. J., and Cole, D. K. (2012) TCR/pMHC Optimized Protein crystallization Screen. *J Immunol Methods* **382**, 203-210

50. Winter, G. (2010) xia2: an expert system for macromolecular crystallography data reduction. *Journal of Applied Crystallography* **43**, 186-190

51. Winn, M. D., Ballard, C. C., Cowtan, K. D., Dodson, E. J., Emsley, P., Evans, P. R., Keegan, R. M., Krissinel, E. B., Leslie, A. G., McCoy, A., McNicholas, S. J., Murshudov, G. N., Pannu, N. S., Potterton, E. A., Powell, H. R., Read, R. J., Vagin, A., and Wilson, K. S. (2011) Overview of the CCP4 suite and current developments. *Acta Crystallogr D Biol Crystallogr* **67**, 235-242

52. Adams, P. D., Afonine, P. V., Bunkoczi, G., Chen, V. B., Davis, I. W., Echols, N., Headd, J. J., Hung, L.-W., Kapral, G. J., Grosse-Kunstleve, R. W., McCoy, A. J., Moriarty, N. W., Oeffner, R., Read, R. J., Richardson, D. C., Richardson, J. S., Terwilliger, T. C., and Zwart, P. H. (2010) PHENIX: a comprehensive Python-based system for macromolecular structure solution. *Acta Crystallographica Section D* **66**, 213-221

53.   Emsley, P., and Cowtan, K. (2004) Coot: model-building tools for molecular graphics. *Acta Crystallographica Section D* **60**, 2126-2132

54.   Hekkelman, M. L., Te Beek, T. A., Pettifer, S. R., Thorne, D., Attwood, T. K., and Vriend, G. (2010) WIWS: a protein structure bioinformatics Web service collection. *Nucleic Acids Res* **38**, W719-723

55.   Anandakrishnan, R., Aguilar, B., and Onufriev, A. V. (2012) H++ 3.0: automating pK prediction and the preparation of biomolecular structures for atomistic molecular modeling and simulations. *Nucleic Acids Res* **40**, W537-541

56.   Maier, J. A., Martinez, C., Kasavajhala, K., Wickstrom, L., Hauser, K. E., and Simmerling, C. (2015) ff14SB: Improving the Accuracy of Protein Side Chain and Backbone Parameters from ff99SB. *J Chem Theory Comput* **11**, 3696-3713

57.   Salomon-Ferrer, R., Gotz, A. W., Poole, D., Le Grand, S., and Walker, R. C. (2013) Routine Microsecond Molecular Dynamics Simulations with AMBER on GPUs. 2. Explicit Solvent Particle Mesh Ewald. *J Chem Theory Comput* **9**, 3878-3888

58.   Stamogiannos, A., Maben, Z., Papakyriakou, A., Mpakali, A., Kokkala, P., Georgiadis, D., Stern, L. J., and Stratikos, E. (2017) Critical Role of Interdomain Interactions in the Conformational Change and Catalytic Mechanism of Endoplasmic Reticulum Aminopeptidase 1. *Biochemistry* **56**, 1546-1558

59.   Humphrey, W., Dalke, A., and Schulten, K. (1996) VMD: Visual molecular dynamics. *Journal of Molecular Graphics* **14**, 33-38

60.   Kumar, S., Rosenberg, J. M., Bouzida, D., Swendsen, R. H., and Kollman, P. A. (1992) THE weighted histogram analysis method for free-energy calculations on biomolecules. I. The method. *Journal of Computational Chemistry* **13**, 1011-1021

FOOTNOTES

The abbreviations used are: MHC I, Major Histocompatibility Complex class I; pMHC I, peptide-bound MHC I; ER, endoplasmic reticulum; ERAP1, ER aminopeptidase 1; TAP, transporter associated with antigen processing; Tpn, tapasin; PLC, peptide loading complex; CTL, cytotoxic T lymphocyte; HC, heavy chain; β_2m, beta-2-microglobulin; SCT, single-chain trimer; SL8, SIINFEKL; IL7, IINFEKL; MD, molecular dynamics; PMF, potential of mean force

TABLE 1. Data collection statistics and refinement for the SL8-K^b single chain trimers.

Protein PDB ID	wild type 5OQF	E63A 5OQI	K66A 5OQH	W167A 5OQG
Space group	P 21	P 21	P 21	P 21
Unit cell				
a, b, c (Å)	66.65, 90.08, 89.33,	67.13, 90.19, 89.45,	66.43, 89.32, 89.40,	66.43, 89.64, 89.45,
α, β, γ (°)	90.00, 111.23, 90.00	90.00, 111.22, 90.00	90.00, 111.24, 90.00	90.00, 111.24, 90.00
Upper resolution limit (Å)	2.27	2.40	2.05	1.90
Lower resolution limit (Å)	90.08	42.52	39.36	61.51
Multiplicity	2.8	3.8	3.8	7.5
Completeness (%)	98.6	97.9	98.2	99.8
R-merge (%)	7.7	10.3	7.4	7.0
Mean (I)/sd (I)	9.8 (2.0)	11.6 (2.1)	9.9 (2.4)	13.8 (2.8)
Reflections	44965	38114	59972	76876
R-factor	0.199	0.198	0.204	0.188
R-free	0.250	0.259	0.241	0.239
Crystallization conditions	Am sulfate, PEG 8K, Na cacodylate pH 6.0	PEG 4K, Na cacodylate pH 6.5	Am sulfate, PEG 8K, Na cacodylate pH 6.0	Am sulfate, PEG 8K, bis-tris pH 6.5
Average all-atom B-factor (Å^2)	38.0	38.0	35.0	38.0
RMSD$^{C\alpha}$ against wt (Å) for chain A / B		0.514 / 0.413	0.266 / 0.404	0.355 / 0.391
Peptide RMSD$^{C\alpha}$ against WT (Å) for chain A / B		0.268 / 0.223	0.268 / 0.179	0.180 / 0.248
RMSD$^{C\alpha}$ against 2QRT (Å) for chain A / B	0.401 / 0.449	0.522 / 0.445	0.375 / 0.295	0.414 / 0.388
Peptide RMSD$^{C\alpha}$ against 2QRT (Å) for chain A / B	0.239 / 0.394	0.329 / 0.389	0.145 / 0.344	0.192 / 0.280

FIGURE LEGENDS

FIGURE 1. Disulfide trap single chain trimer structure. (*A*) Ribbon representation of the WT-SCT color-coded with green for the HC and blue for the β_2m domain. SL8 is shown with orange C sticks and the linker between SL8 and β_2m (PL) with purple C atoms. PL residues that were not resolved in our X-ray structures and the linker between β_2m and the K^b heavy chain (BL) are indicated by purple dashed lines. The N- and C-termini of HC and β_2m are indicated as hc1–hc276 and β1–β99, respectively. (*B*) Close-up view of the peptide binding domain illustrating SL8 (orange C, blue N, red O), the PL residues resolved (purple C) and the engineered residue Y84C (cyan C, yellow S) that comprises the disulfide trap with the PL residue C10. (*C*) Schematic organization of the WT-SCT showing the residue numbering of each domain (upper) and the corresponding numbering in the PDB files (lower). Disulfide bridges are shown with yellow lines and the three mutated positions are indicated.

FIGURE 2. Cell surface expression of WT and A-pocket variant SCT. HeLa and HeLa ERAP1 KO (E1KO) cells were transfected with WT-SCT, A-pocket variants E63A-, K66A- or W167A-SCT and cell surface expression assessed using the SIINFEKL/K^b-specific antibody 25-D1.16 or anti-mouse β_2m. (A) 25-D1.16 and anti-mouse β_2m staining of HeLa cells transfected with either WT-SCT or IINFEKL (IL7)-SCT. (B) CRISPR/Cas9 knockout of ERAP1 in HeLa cells. (C) 25-D1.16 staining of HeLa E1KO cells transfected with WT or A-pocket variant SCT.

FIGURE 3. The effect of A-pocket mutation on SCT peptide binding groove structure. Close-up view of the peptide binding domain of the WT-SCT crystal structures illustrating hydrogen bonding interactions between S(P_1), I(P_2) and the mutated residues in (*A*) WT, (*B*) E63A, (*C*) K66A and (*D*) W167A variants. Solvent molecules that mediate conserved hydrogen bonds are shown as red spheres (Wat1/2), while yellow spheres indicate waters that fill a space created by the mutated residue. The second alternative conformation of the N(P_4) side chain resolved in the W167A-SCT (*D*) is highlighted with green C atoms.

FIGURE 4. A-pocket mutations allow trimming of SIINFEKL peptide bound to K^b. HeLa ERAP1 KO cells were transfected with WT-SCT, A-pocket variants E63A-, K66A- or W167A-SCT with or without the overexpression of ERAP1. Cell surface expression of SCT was assessed using the SIINFEKL/K^b-specific antibody 25-D1.16 or anti-mouse β_2m. (A, B) 25-D1.16 staining of HeLa E1KO cells transfected with WT or A-pocket variant SCT with or without expression of ERAP1. (C) Cell surface expression of SCT assessed by anti-mouse β_2m following transfection with ERAP1 (red = -ERAP1, blue = +ERAP1, filled histogram = negative control). The data is pooled from at least 3 experiments (*** = p <0.001, ** = p <0.01, * = p <0.05, ns = not significant).

FIGURE 5. ERAP1 reduces the stimulation of B3Z by single chain trimer MHC molecules.
HeLa and HeLa E1KO cells were transfected with WT-SCT, A-pocket variants E63A-, K66A-, W167A- or IINFEKL-SCT with or without overexpression of ERAP1. (A) A representative experiment showing the stimulation of B3Z T cell hybridomas by the transfected SCT. (B) The relative B3Z response of WT- and E63A-SCT in the presence or absence of ERAP1 in HeLa E1KO cells. (C) The relative B3Z response of WT- and E63A-SCT in the presence or absence of additional ERAP1 in HeLa cells. The data is pooled from at least 3 experiments (** = p <0.01, * = p <0.05).

FIGURE 6. MD simulations of single chain trimers. (*A*) Snapshot of the W167A-SCT peptide binding domain from the unrestraint MD simulations exhibiting dissociation of the N-terminal half of SL8. The dashed arrow indicates the distance between S(P_1) and the bottom of the A pocket (δ) that was employed as the reaction coordinate in free energy calculations. (*B*, *C*) Plots of the free energy change as a function of distance (δ) obtained from umbrella sampling calculations employing (*B*) the four SCTs and (*C*) the four

16

corresponding untethered SL8/K^b complexes. Error bars indicate the standard deviation at each point as extracted from four independent runs.
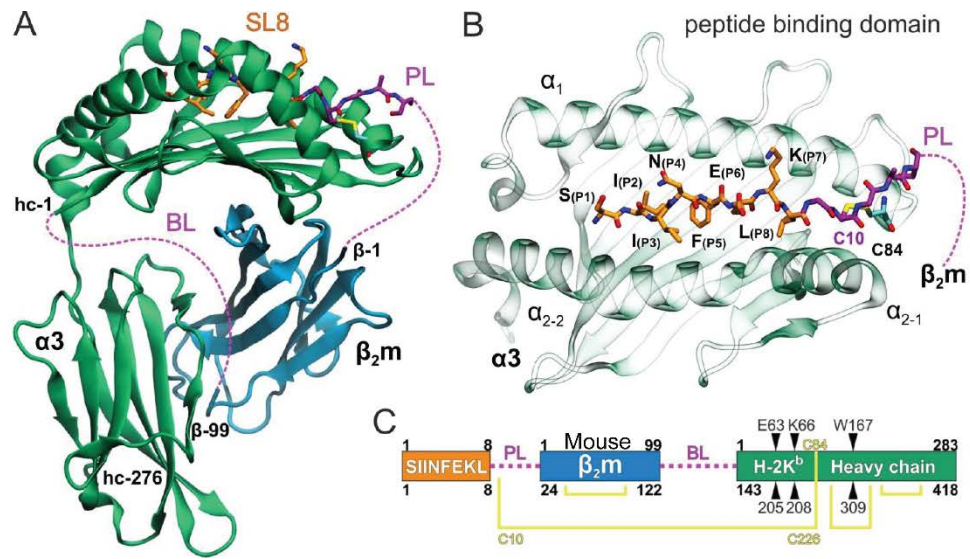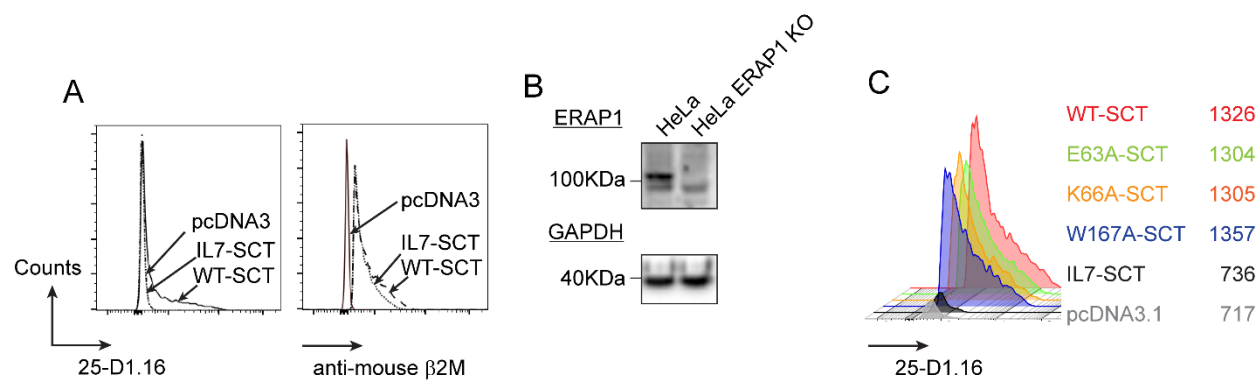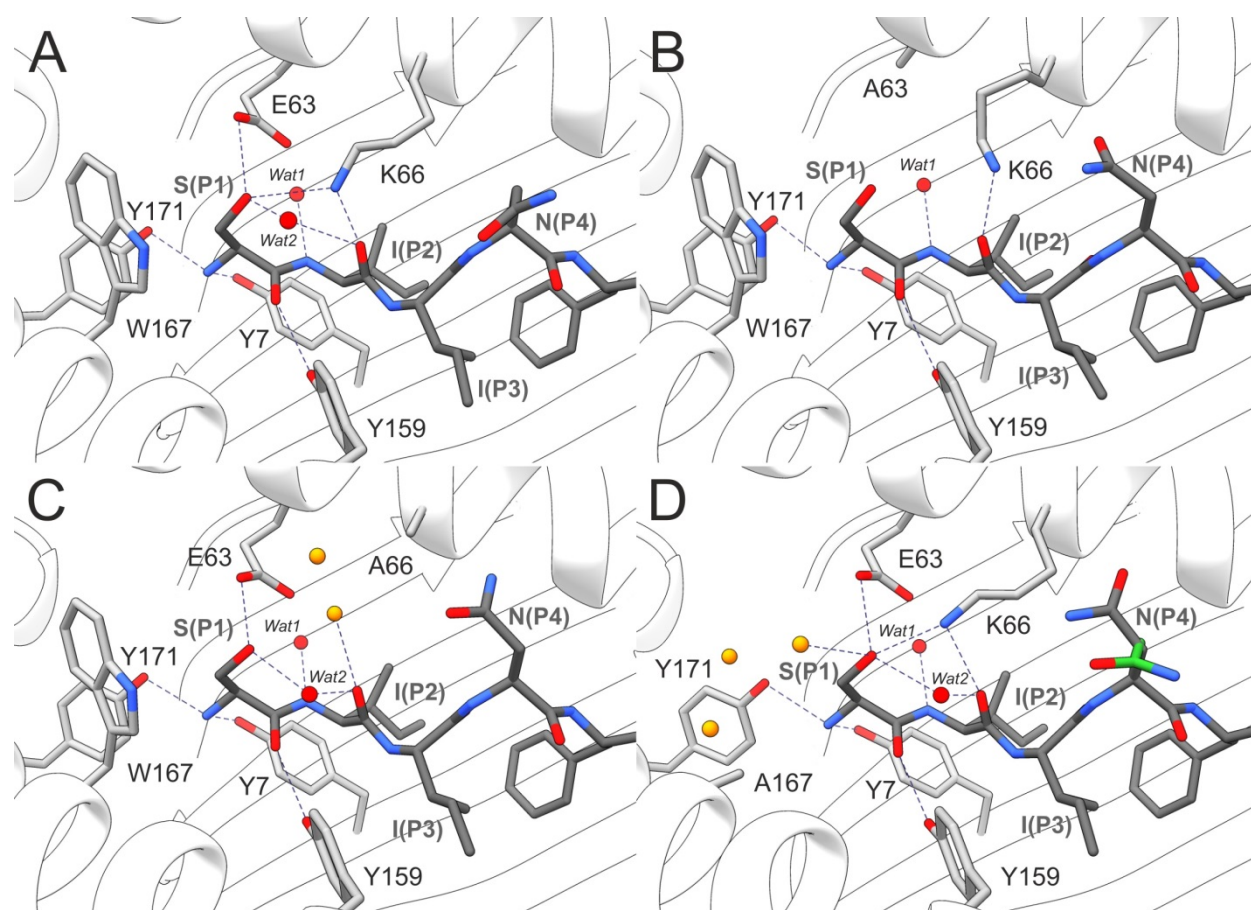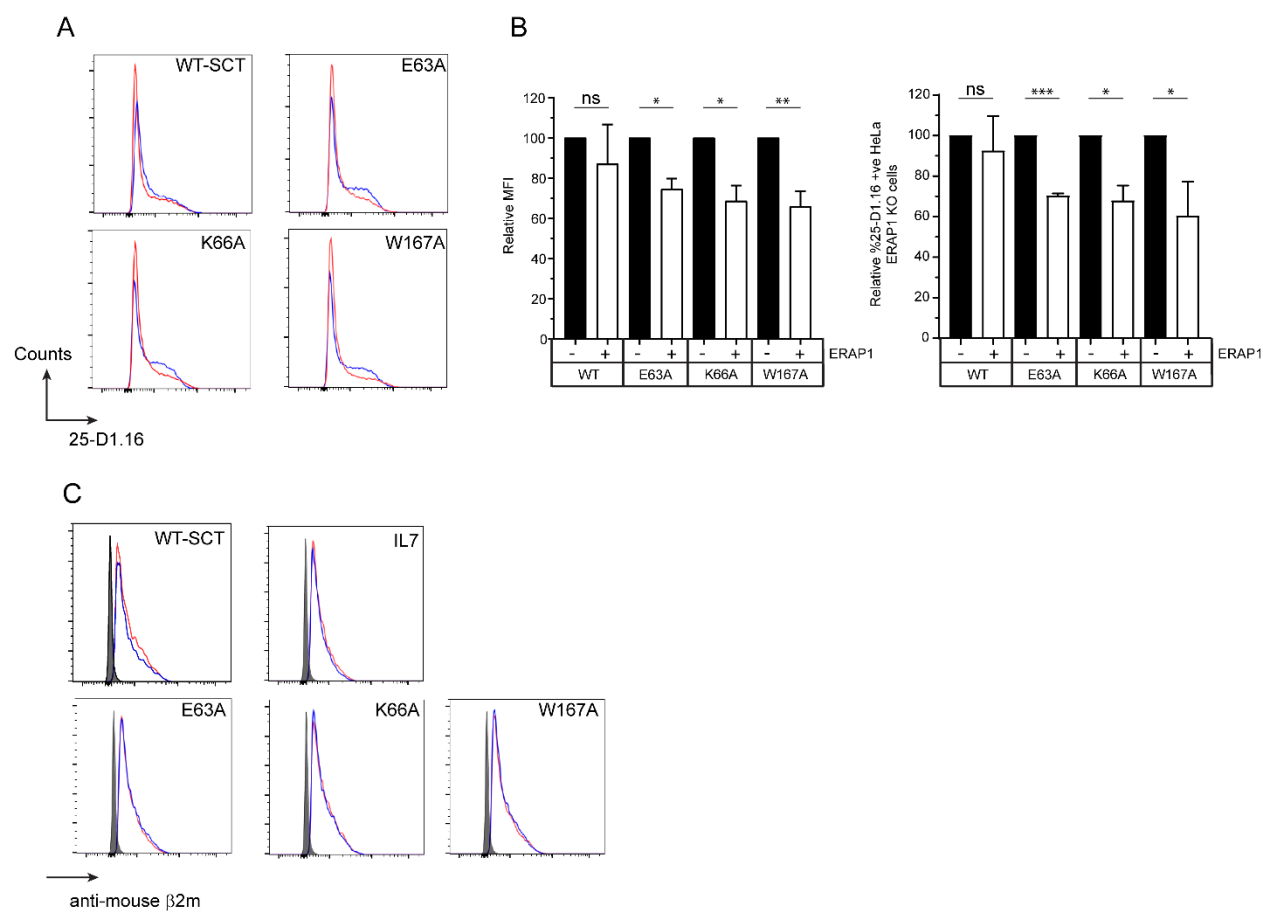
FIGURE 1.

FIGURE 2.

A

Counts

25-D1.16   anti-mouse β2M

pcDNA3
IL7-SCT
WT-SCT

pcDNA3
IL7-SCT
WT-SCT

B

ERAP1   HeLa   HeLa ERAP1 KO

100KDa —

GAPDH

40KDa —

C

25-D1.16

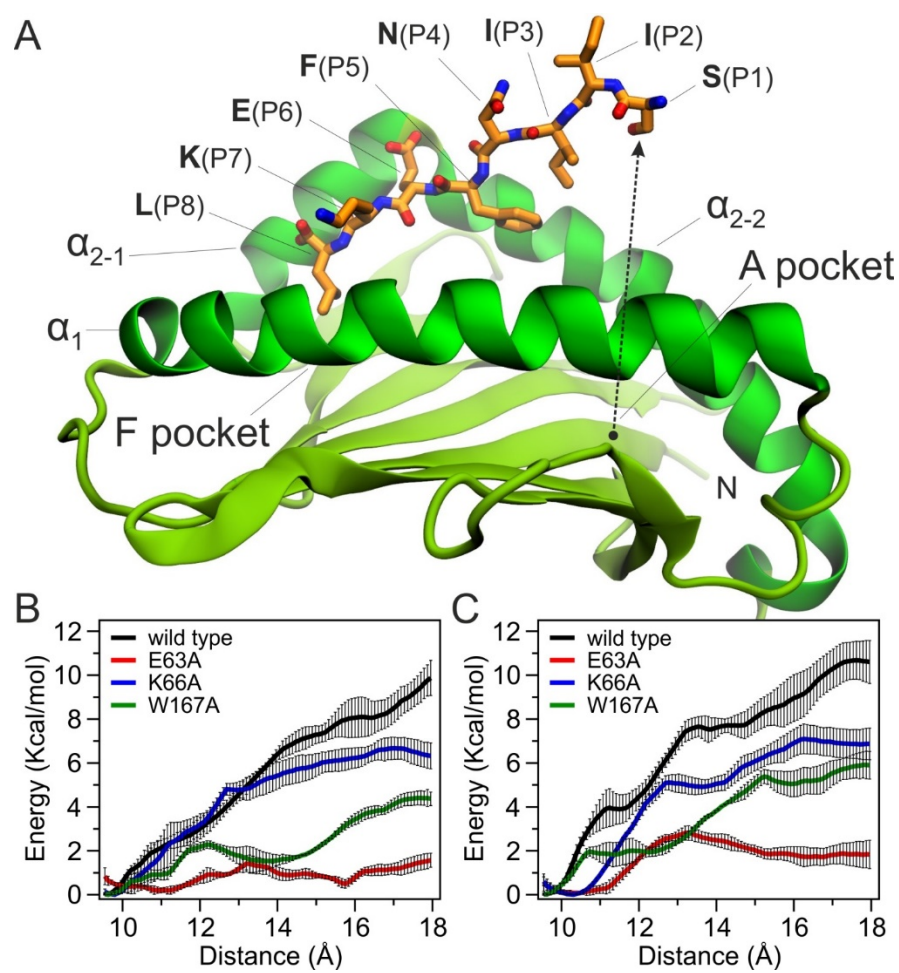|	
WT-SCT	1326
E63A-SCT	1304
K66A-SCT	1305
W167A-SCT	1357
IL7-SCT	736
pcDNA3.1	717

FIGURE 3.

FIGURE 4.

21

FIGURE 5.

A
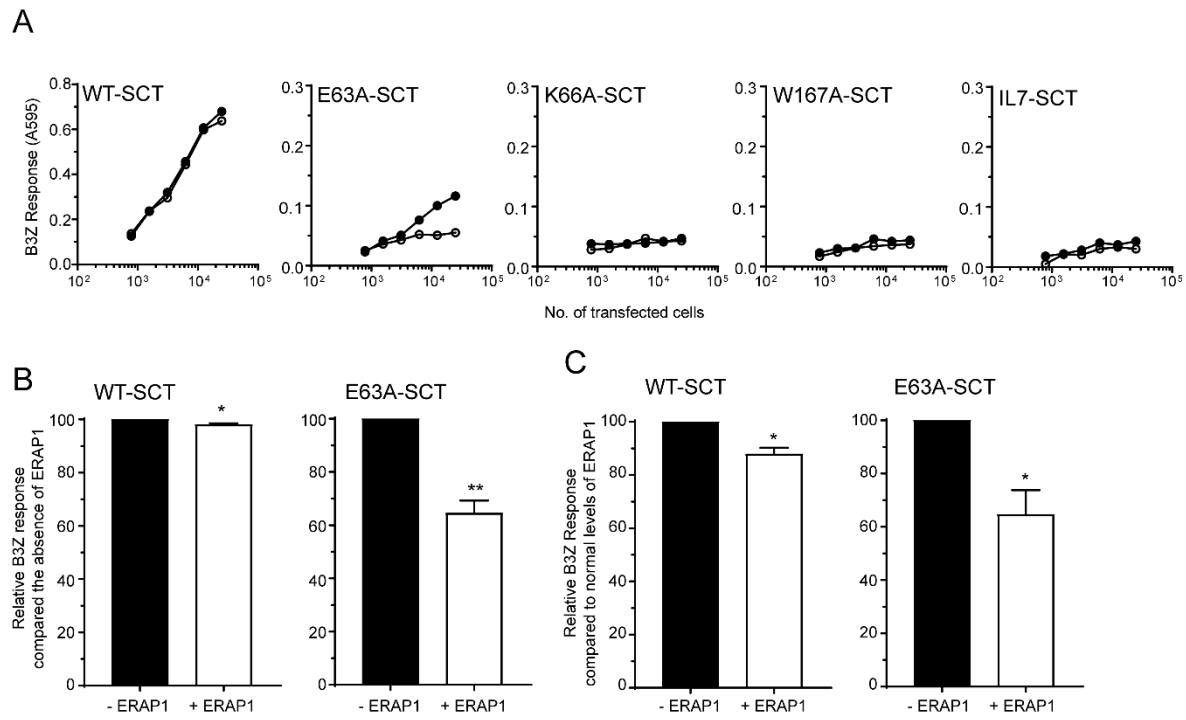
FIGURE 6.

The partial dissociation of MHC class I bound peptides exposes their N terminus to trimming by endoplasmic reticulum aminopeptidase 1

Athanasios Papakyriakou, Emma Reeves, Mary Beton, Halina Mikolajek, Leon Douglas, Grace Cooper, Tim Elliott, Jörn M Werner and Edward James

Access the most updated version of this article at doi: 10.1074/jbc.RA117.000313

Alerts:
- When this article is cited
- When a correction for this article is posted

Click here to choose from all of JBC's e-mail alerts